J Mater Sci: Mater Med (2011) 22:705–720
DOI 10.1007/s10856-010-4221-3

Macro-to-micro porous special bioactive glass and ceftriaxone–sulbactam composite drug delivery system for treatment of chronic osteomyelitis: an investigation through in vitro and in vivo animal trial

Biswanath Kundu · Samit Kumar Nandi · Sudip Dasgupta · Someswar Datta · Prasenjit Mukherjee · Subhasis Roy · Aruna Kumari Singh · Tapan Kumar Mandal · Partha Das · Rupnarayan Bhattacharya · Debabrata Basu

Received: 1 September 2010 / Accepted: 19 December 2010 / Published online: 8 January 2011

Abstract A systematic and extensive approach incorporating in vitro and in vivo experimentation to treat chronic osteomyelitis in animal model were made using antibiotic loaded special bioactive glass porous scaffolds. After thorough characterization for porosity, distribution, surface charge, a novel drug composite were infiltrated by using vacuum infiltration and freeze-drying method which was subsequently analyzed by SEM–EDAX and studied for in vitro drug elution in PBS and SBF. Osteomyelitis in rab bit was induced by inoculation of *Staphylococcus aureus* and optimum drug-scaffold were checked for its efficacy over control and parenteral treated animals in terms of histopathology, radiology, in vivo drug concentration in bone and serum and implant-bone interface by SEM. It was optimized that 60P samples with 60–65% porosity (bimodal distribution of macro- to micropore) with average pore size $\sim$60 μm and higher interconnectivity, moderately high antibiotic adsorption efficiency ($\sim$49%) was ideal. Results after 42 days showed antibiotic released higher than MIC against S. aureus compared to parenteral treatment (2 injections a day for 6 weeks). In vivo drug pharmacokinetics and SEM on bone-defect interface proved superiority of CFS loaded porous bioactive glass implants over parenteral group based on infection eradication and new bone formation.

B. Kundu · S. Dasgupta · S. Datta · D. Basu (✉)
Bioceramics and Coating Division, Central Glass and Ceramic Research Institute, 196, Raja S. C. Mullick Road, Kolkata 700028, India
e-mail: dbasu1960@rediffmail.com

S. K. Nandi (✉) · P. Mukherjee · S. Roy
Department of Veterinary Surgery and Radiology, West Bengal University of Animal and Fishery Sciences, 37 and 68, Kshudiram Bose Sarani, Kolkata 700037, India
e-mail: samitnandi1967@gmail.com

A. K. Singh · T. K. Mandal
Department of Veterinary Pharmacology and Toxicology, West Bengal University of Animal and Fishery Sciences, Kolkata, India

P. Das
Department of Anatomy and Histology, West Bengal University of Animal and Fishery Sciences, Kolkata, India

R. Bhattacharya
Department of Plastic Surgery, R. G. Kar Medical College and Hospital, Kolkata, India

Abbreviations

HAp	Hydroxyapatite
β-TCP	Beta-tri calcium phosphate
SEM–EDAX	Scanning electron microscopy–energy dispersive analysis of X-ray
HPLC	High performance liquid chromatography
PBS	Phosphate buffered saline
SBF	Simulated body fluid
PMMA	Poly-methylmethacrylate
MIC	Minimum inhibitory concentration
CFT	Ceftriaxone sodium
SUL	Sulbactam sodium
CFS	Combination of CFT and SUL drug
XRD	X-ray diffraction
FTIR	Fourier-transformed infrared spectroscopy
FESEM	Field emission scanning electron microscopy
ASTM	American Society for Testing and Materials
CFA	Colony forming unit
RBC	Red blood cell

1 Introduction

Treatment of orthopaedic infections with antibacterial agents by oral or intravenous route often leads the clinicians to be pessimistic about patient outcome [1]; as the condition is frequently associated with poor vascular perfusion accompanied by infection of the surrounding tissue [2]. Following surgical debridement, it is necessary to maintain a highly effective concentration of the antibiotic in the infected area for a sufficient period of time (usually 4–6 weeks) to allow the healing process to complete [3].

Different antibiotic impregnated implants based on various kinds of carrier materials have been tried [4]. With the growing interest for combination devices that could release drug and as well enhance or support tissue regeneration, approaches with bioactive ceramics have proved to improve the prognosis of orthopaedic infections than polymers used conventionally for novel drug delivery systems [5]. However, recently a new gentamicin-vancomycin-impregnated (2:1) poly-methyl methacrylate (PMMA) coating nail has been introduced as a drug delivery device which could treat bone and intramedullary infections [caused by methicillin-resistant *Staphylococcus aureus* (MRSA)] effectively after surgical debridement and immediate implantation [6]. Porous bioceramic scaffolds made with hydroxyapatite, β-TCP have also proved their suitability in releasing drug and accepting bone ingrowth [7, 8]. Macroporosity with pore diameter above 100 μm is desired to permit bone infiltration, on the other hand, bigger the pore size, faster would be the drug elution from the scaffolds [4]. Pore interconnection is another key factor that dominates bone ingrowth; and high pore interconnectivity is generally obtained by high pore volume [9].

Now, CFT is a broad-spectrum semi-synthetic third-generation cephalosporin with a potent bactericidal activity against a wide range of gram-positive and gram-negative bacteria and SUL is β-lactamase inhibitor. CFS have long been considered the drugs of choice for the treatment of chronic osteomyelitis because of their favorable penetration into poorly vascularized sites of infection, their advantageous bactericidal effects against all probable pathogens of chronic osteomyelitis, and the lack of serious adverse reactions [10].

Studies on effect of macro- and microporosity alongwith pore interconnection on the performance of porous bioactive glass scaffolds are yet to be reported to the best of our knowledge which was used as local drug delivery system. Our previous study on goat indicated bioactive glass scaffolds are at least marginally better osteoinductive compared to HAp and β-TCP scaffolds [11]. Hence, in the present study we reported a porous bioactive glass based drug delivery system and extensively studied its suitability in releasing the drug both in vitro and in vivo for a prolonged time period and supporting new bone formation and hence dead space management. The bioactive glass composition used had been developed earlier in our lab and proved to be bioactive and noncytotoxic in vitro [12]. Ceftriaxone–sulbactam combination was selected as model drugs as the combination of beta-lactam antibiotic with an irreversible β-lactamase inhibitor decrease the MICs of hydrolyzed β-lactams to normal [13] and expands the antimicrobial spectrum to include previously β-lactam resistant microorganisms [14].

2 Materials and methods

2.1 Preparation and characterization of bioactive glass powder

A composition of bioactive glass powders was prepared using different raw materials as source of network former and modifiers. The raw materials include silica (SiO_2), calcium carbonate ($CaCO_3$), dry soda ash (Na_2CO_3), decahydrated borax ($Na_2B_4O_7{\cdot}10H_2O$), titania (TiO_2), di-ammonium hydrogen ortho-phosphate (all chemicals were analytical grade from M/s SD Fine-Chem Limited, India). The powder was prepared by following usual glass melting (1400°C) procedures, details of which could be found elsewhere [11, 15]. Final chemical composition of this glass, which was used subsequently for fabrication of porous scaffolds, is given in Table 1.

Surface charge in terms of zeta potential of the as-prepared powder (1400°C) as well as powders fired at 725°C/5 min (optimized sintering temperature of porous scaffolds) was also estimated for indirect estimation of interaction between these particles and CFS. Zeta potential of these particles was determined using suspensions containing 0.01% (w/v) of such particles in a 10^{-3} M KCl solution. The measurements were taken as a function of pH at 20°C. The pH was adjusted with 0.1 M KOH and 1 N HCl solutions for basic and acidic conditions, respectively.

Table 1 Final composition of the bioactive glass

Composition	wt%
SiO_2	43.70
CaO	19.20
P_2O_5	5.46
B_2O_3	9.40
Na_2O	22.24

2.2 Fabrication and characterization of porous scaffolds

First, the ground (−52 British Standard Sieve, i.e. <296 μm) bioactive glass powder was intimately mixed with appropriate quantity of naphthalene powder (Scintillation grade, SD Fine-Chem Limited, India) by repeated sieving in a sieve shaker (Retsch, AS200, Germany). Porous units were fabricated by modification of a process, developed by us earlier [16]. In the present investigation, naphthalene was added at two different percentages for the scaffold formulation, viz., 50 and 60%, (hereinafter the same designated as 50P and 60P). The powder mix was subsequently compacted at a pressure of 150 MPa (for 40 s) by cold-isostatic pressing (EPSI N.V.; SO 10036, Belgium) to form cylindrical shaped green specimens. Specimens having required dimensions suitable for further characterization were machined using a manual lathe machine. By heating up to 80°C, the naphthalene was driven off from the green specimens with care to prevent cracking, at this stage. Finally, the green and now fragile specimens were directly fired at 725°C (kept for 5 min at this temperature) in a platinum crucible using a small furnace (Vita Vacumat 40T, Germany) with air atmosphere. Physical properties including apparent or open porosity, closed porosity and bulk density of the sintered porous specimens were measured by Archimedes' principle (water displacement method) and calculated by the usual methods. For calculation of closed porosity percent, powder density of the bioactive glass powder was taken as 2.7 g/cm^3 [17].

Microstructure, pore size, shape and morphology were observed by field emission scanning electron microscopy (FESEM) (Carl Zeiss, Supra 35 VP, Germany) on one side of the flat-parallel surface. Image analysis was carried out to calculate the pore size distribution (Perfect Screen Ruler 2.0, Styopkin Software, USA). More than 250 linear measurements were taken from each micrograph and converted to their actual dimension from the corresponding tag of each microstructure. Histograms thus obtained were plotted as function of pore size ranges. The average pore sizes were also determined.

2.3 Fabrication and characterization of drug impregnated scaffolds

We have used a combination of two drugs CFT and SUL in 2:1 ratio. Five numbers of samples for each kind of porous scaffolds were soaked in a solution of CFS (500 mg/ml concentration) prepared in ultra-pure water (Milli-Q Academic Century, ZMQS50001, China) and subjected to a vacuum of 10 mmHg for at least 30 min. The samples were further freeze dried (Eyela, FDU-2200, Japan) and checked for adsorption efficiency. This was expressed as percentage (the change in weight of bioactive glass scaffold before and after drug impregnation divided by the weight before impregnation) [18].

A section of these CFS impregnated porous blocks were characterized for microstructural evolution using SEM (Leo 430i Steroscan, UK). Depending on the samples' composition, microstructures were taken either in secondary electron or back-scatter electron mode. The samples were mounted and sputter-coated with a thin film of carbon prior testing. For assessment of the compositional variation along the interface between pore surface and drug, EDAX (vacuum: 1.14×10^{-6} mbar, beam current of electron gun: 1.0 nA, spot size: 520 nm, working distance: 8.5–9 mm, SiLi detector and collection time: 45 s) were taken. Depending on the microstructure observed, line-scan of EDAX was performed for compositional variation and compared with the said microstructure.

2.4 In vitro drug release studies

In vitro drug elution studies were performed in two liquid mediums PBS and SBF. PBS used was a solution of salts as NaCl (137 mM), KCl (2.7 mM), Na_2HPO_4 (10 mM), KH_2PO_4 (1.8 mM) with a pH of 7.4 while SBF was prepared in accordance to Kokubo et al. with ionic concentrations equal to human blood plasma [19]. CFS impregnated scaffolds were placed in test tubes containing 3 ml of liquid medium and stored in a thermostatic chamber at ~37.4°C. After each day up to 7 days and each week subsequently up to 42 days, the samples were removed and transferred to a new tube containing 3 ml of fresh liquid medium. The liquid mediums containing the released CFS were stored at −80°C until analysed. After filtration, the amount of CFS release were determined by HPLC (Shimadzu, SPD-MIOA, Japan) fitted with binary pump (LC-20 AT), diode array detector. Similar procedures were followed for obtaining the assays up to 42 days. The conditions for HPLC were as follows: For determination of CFT, the mobile phase was composed of HPLC grade water: acetic acid: acetonitrile ~70:5:25 with flow rate 1 ml/min and detection wavelength 254 nm. The separation was carried out using an RPC_{18} pH stable column (Phase Separations, Norwalk, CT), 15 cm long. For determination of SUL, the mobile phase was a mixture of buffer and acetonitrile in a volume ratio of 88:12 (the buffer was a solution of 0.1 M KH_2PO_4, tetra-butyl-ammonium hydroxide and 0.1 M phosphoric acid). The flow rate was 1.5 ml/min with detection wavelength of 313 nm. Percent yield of CFS was expressed as the total amount of released antibiotic divided by the amount of CFS held in the samples before the start of elution in PBS and SBF separately [18].

2.5 Bacterial isolate

Staphylococcus aureus (coagulase positive) from an animal with chronic osteomyelitis was used for development of experimental model in rabbit. Pure cultures of the bacteria were obtained on blood agar at 37°C and standardized suspensions (3×10^6 CFU/ml) were prepared in saline. This sample (1 ml) was introduced into the medullary cavity of rabbit tibiae and confirmed successful induction of osteomyelitis by *S. aureus* based on mannitol salt agar test. Twenty-one (21) days of post inoculation, the swab specimen was collected from the infected site from animals of all groups and was streaked on mannitol 10% salt agar slant and incubated at 37°C for overnight. From single colony, bacterial growth was collected and stained by Gram's staining method. At the time that the animals were sacrificed (12, 21 and 42 days for group II and III animals), swab specimen was collected from the implanted site of bone and similarly, inoculated to mannitol 10% salt agar and incubated at 37°C for overnight.

2.6 In vivo studies

According to the model of Norden [20], osteomyelitis was induced in the right tibia of 24 (twenty-four) nos. of adult New Zealand white rabbits (2.5–3 kg body weight). The proximal part of the tibia was exposed anteriorly after anaesthesia with Nembutal 0.5 mg/kg IV (Thiopentone sodium, Thiosol®, Neonlab, Mumbai, India), and a hole was drilled through the cortex into the medullary cavity using a 1.2 mm diameter dental burr. 1 ml of *S. aureus* suspension containing approximately 3×10^6 CFU/ml was injected into the drilled medullary cavity and the hole was sealed with bone wax to prevent bacterial leakage into the surrounding soft tissues. The animals were monitored after surgery. All the animals received standard postoperative pain medication (Carprofen; 4 mg/kg of body weight) for 3 days. The animals which developed osteomyelitis after 3 weeks of inoculation were only considered for present study. By using the previous surgical approach, the proximal tibia was exposed and bone defects were created by micromotor dental drill. CFS impregnated bioactive glass blocks were implanted in the defect area of infected bone and same postoperative management was followed. All the animal experimentations were carried out following the procedures conforming to the standards of the Institutions Animal Ethical Committee of the West Bengal University of Animal and Fishery Sciences, India. The 24 animals were divided into 3 Groups hereinafter would be designated as group I, II and III. The details of the experimentation with these animals are given in Table 2. All the samples and study parameters were obtained on 12, 21 and 42 days post osteomyelitis. Animals were pharmacologically euthanised under general anaesthesia after 42 days. The implanted bone/antibiotic impregnated bioactive glass implants were collected and then thoroughly washed implants were fixed in 10% formalin for 7 days and subsequently decalcified in Goodling and Stewart's fluid containing formic acid 15 ml, formalin 5 ml and distilled water 80 ml solution. Decalcification was confirmed by flexible and transparent section easily penetrable with pin. Decalcified bone specimens were first embedded with paraffin and sections were cut (3–4 mm thick) with rotary microtome (HM 360, Microm, Germany). Hematoxyline and eosin stained decalcified cross sections were considered for histological examinations. Histological images were analyzed digitally as par different cellular events occurred with time and following features were noted and

Table 2 Design of experiment for in vivo animal experimentation

Groups	No. of animals	Implant	Days of experiment	Experiment
Group I	6	Not given	After 21 days	Six animals were sacrificed for histological, radiographic and microbiological examination to confirm development of osteomyelitis
Group II	9	CFS injection parenterally (15 mg/kg, bid) twice daily for 6 weeks	12 days	Three animals were sacrificed for histological and estimation of drug concentration in bone and serum
			After 21 days	Three animals were sacrificed for histological and estimation of drug concentration in bone and serum
			After 42 days	Three animals were sacrificed for histological and estimation of drug concentration in bone and serum
Group III	9	Ceftriaxone–sulbactam impregnated bioactive glass blocks	12 days	Three animals were sacrificed for histological and estimation of drug concentration in bone and serum
			After 21 days	Three animals were sacrificed for histological and estimation of drug concentration in bone and serum
			After 42 days	Three animals were sacrificed for histological, radiographic, and estimation of drug concentration in bone and serum

rated (from 4 to 1) for absent (4), scanty/mild (3), moderate (2) and abundant (1): (i) degenerative changes, (ii) fibrovascular proliferation, (iii) infiltration with mononuclear cells, (iv) osteoclastic activity, (v) fibropurullent reaction, (vi) mucin deposit, (vii) vascularity and (viii) presence of giant cells.

Radiographic images (300 mA medical diagnostic X-ray machine, M.E. X-Ray, India) of the subjected bones were taken under direct radiographic magnification. Similarly, radiographic images were semi-quantitatively digitized for different events of bone formation/destruction including (i) periosteal reaction, (ii) visible bone defect, (iii) endosteal reaction, (iv) radiodensity, (v) resorptive changes and (vi) cortical continuity and rated as par a scoring from 1 to 4 [marked (1), moderate (2), mild (3) and absent (4)] for (i)–(iii) and from 4 to 1 [marked (4), moderate (3), mild (2) and absent (1)] for (iv)–(vi). All parameters for both histopathology and radiology were analyzed by SPSS (v. 14) software with one-way ANOVA (analysis of variance) analysis. Blood samples from the ear vein and pulverized, homogenized, centrifuged supernatant fluid from cortico-cancellous portion of tibia (after removing bone marrow) were collected for estimation of antibiotic (separately for CFT and SUL) by HPLC techniques by the methods described earlier. The results were expressed as means ± standard deviations.

Specimens were also collected for SEM analysis from the cortical part of the bone of animals from all the three groups after 42 days; while from group III, samples were also collected after 21 days, post-operatively. For SEM specimens, 5% glutaraldehyde phosphate solution was used for fixing the samples, washed twice for 30 min with PBS (pH 7.4) and distilled water, dehydrated in a series of graded ethanol followed by final drying with hexamethyldisilizane (HMDS). A gold conductive coating was given by ion sputtering (JEOL ion sputter, Model JFC 1100, Japan) at 7–10 mA and 1–2 kV for 5 min. The resin mounted sample surfaces were then examined under SEM (JEOL JSM 5200 model, Japan) after proper alignment.

3 Results

3.1 Characterization of the powders

Details of the characterization of both powders and scaffolds could be found elsewhere [11, 15]. In summary, both X-ray diffraction (XRD) and Fourier transformed infra-red spectroscopy (FTIR) confirmed the amorphous nature and prevalence of Si–O functional groups. It was also found that the relative positions of the hump as seen from the XRD pattern were unchanged with temperature. There was no incipient formation of crystals, which was undesirable for actual in vivo applications. FTIR spectra showed well-defined transmission bands characteristic of the samples prepared at 1400°C and fabricated at 725°C/5 min with sharp split bands. All the transmission spectra showed a broad band at around 3455 cm^{-1} which was assigned to OH^- group or silanol (Si–OH) group. There were bands at around 1094, 776 and 416 cm^{-1} which were due to Si–O–Si asymmetric stretching of bridging oxygen atoms within the tetrahedra, Si–O–Si symmetric stretching of bridging oxygen atoms within the tetrahedral and Si–O–Si bending, respectively. This observation was also correlated the observation of Hench.

3.2 Characterization of porous scaffolds

Physical parameters such as percent open and closed porosity, bulk density of the porous bioactive glass scaffolds measured by Archimedes' water displacement method are given in Table 3. It was found that the increase in naphthalene content in the formulation resulted higher porosity and hence lower bulk density in 60P samples. Increase of naphthalene by 10% resulted in increment of open porosity by ~6%. SEM microstructures of the porous body fabricated using different percentage of naphthalene (50P and 60P) are presented in Fig. 1a and b, respectively. Histograms based on image analysis were plotted as function of pore size ranges and are presented in Fig. 2a and b for 50P and 60P samples, respectively. The microstructures were more non-uniform in 50P than 60P samples with high interconnectivity of pores for the later. 50P samples had granular microstructures with large amount of micropores. For the both the cases monomodal distribution of pores was noticed. Both micro-pores (<50 μm) and macro-pores (>50 μm) were evidenced from micrograph with higher amount of macro-pores in 60P samples than the 50P one. The average pore size for both these kinds of samples were calculated and found to be ~18.1 and 60.2 μm for 50P and 60P samples, respectively. Sub-surface interconnections were found in the range from 25 to 95 μm throughout the microstructures of 60P samples and about 15–50 μm for 50P samples. Both the microstructures were mainly amorphous character with absence of grain boundary between particles. Micropores were restricted on the surface with pore closures could be seen on the sub-surface of 50P samples. In this case, the pores were

Table 3 Physical parameters of the porous scaffolds before drug impregnation

Sample	Bulk density (g/cm^3)	Open porosity (%)	Closed porosity (%)
50P	1.25 ± 0.07	50.89 ± 2.53	9.58 ± 0.05
60P	1.14 ± 0.05	56.67 ± 2.44	7.08 ± 0.05

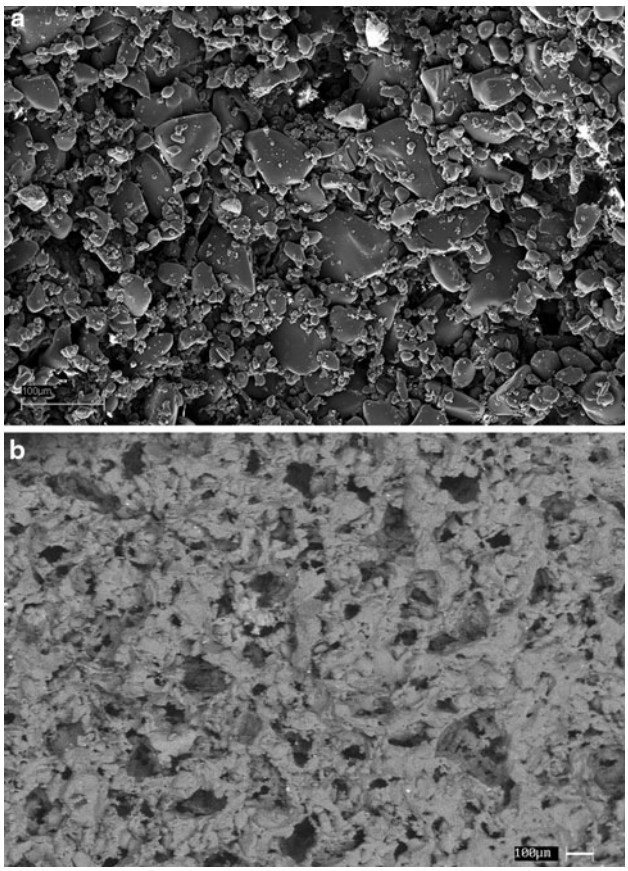

Fig. 1 Microstructure of **a** 50P and **b** 60P sample

moderately interconnected and there was no as such geometry of the pore morphology resembling the escape of naphthalene while dried. On the other hand, better interconnections could be observed for 60P samples with macro-to-micro sized pores for better biological fluid exposure in vivo.

3.3 Characterization of drug loaded porous scaffolds

Adsorption efficiency of the drug CFS for 50P and 60P samples were on an average found to be ~32 and 49%, respectively. Adsorption efficiency actually increased with increase of pore percentage and distribution of pores. Due to increase in the surface area of the pores, the drug adsorption efficiency was also increased for 60P samples. Surface charge in terms of zeta potential for bioactive glass powders fired at 1400°C (powders obtained after glass melting at this temperature) and 725°C (sintering temperature) with varying pH is given in Fig. 3. Bioactive glass had moderately high negative potential throughout the observed pH spectrum and hence could safely be said that in the physiologic pH spectrum it will behave as anionic. At physiological pH, it was found to be ~−21.7 mV for 725°C sintered samples where glass particles at green state

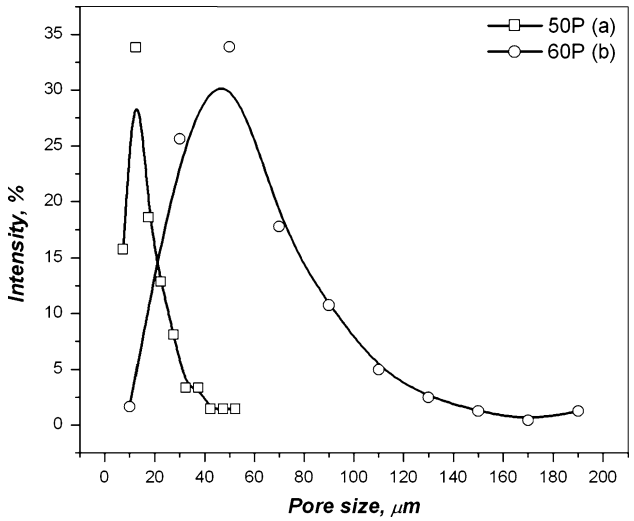

Fig. 2 Histogram to show the pore size distribution of (*a*) 50P and (*b*) 60P sample

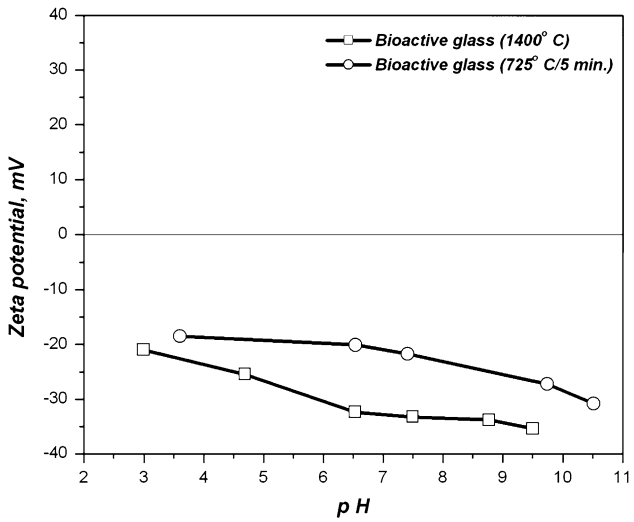

Fig. 3 Variation of zeta potential with pH for as-prepared bioactive glass powder and scaffolds prepared at 725°C

started to coalesce. Moreover, it is the surface charge, which also had a definite role for adsorption to the surface of porous bioactive glass as well as the cohesion between drug CFS and glass.

We have also studied the surface morphology of bioactive glass scaffolds loaded with drug (Fig. 4). The SEM photomicrographs, e.g., in case of 50P, showed microstructure of non-crystalline bioactive glass and its closest approximated drug at the interface infused into the subsurface pores. Cracks were visible at the drug surface only. CFS was intruded through the granular structure of porous bioactive glass. Corresponding EDAX taken at regions marked as A, B and C are given in LHS of Fig. 4 and further crosschecked for compositional variation (if any).

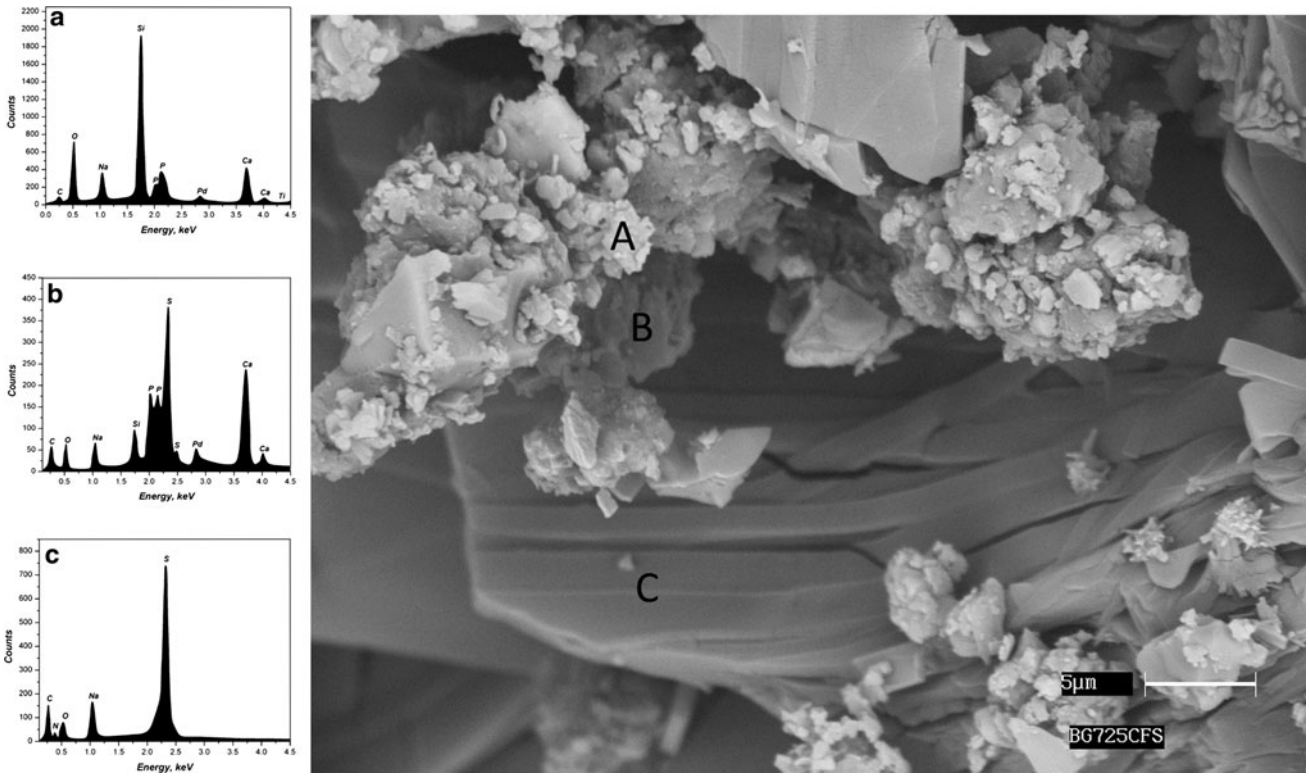

Fig. 4 SEM of the section of CFS impregnated bioactive glass (50P). EDAX were taken at the points *A*, *B* and *C* (LHS)

At point C, there were elements like S (sulphur), Na (sodium), nitrogen (N) and carbon (C) with complete absence of peak corresponding to Si (silicon), Ti (titanium), Ca (calcium), P (phosphorous) and O (oxygen). This indicated the prevalence of drug molecules (CFS) in those areas. White at point A, abundance of later elements could be seen with absence of elements corresponding the drug, which indicated the bioactive glass composition. Point B showed all the elements corresponding the drug and bioactive glass molecule, could infer the interfacial region between theses two. Wherever available, drug molecules were attached on the surface of bioactive glass, might be due to the electrostatic interaction between them. There were no interfacial cracks/gap between glass and infused drug.

3.4 In vitro drug elution study

Release profiles of the drugs CFT and SUL in PBS and SBF were plotted separately in Figs. 5 and 6, respectively. On an average, it was found that the drug yield after 42 days of elution in contact with PBS were ~46.3% and 30.2% for 50P and 60P samples respectively. In general, there was a high release of drugs observed initially from all the samples followed by a much restricted release profile. There was ~0.88 and 0.57 mg/ml of CFT and 0.16 and 0.11 mg/ml of SUL release in the very first day for two

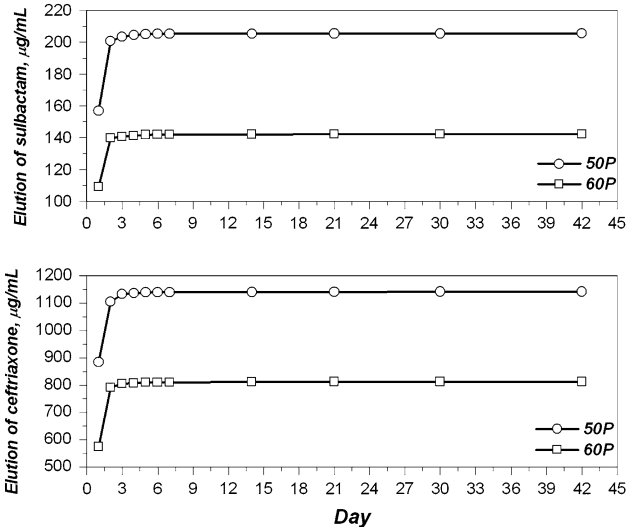

Fig. 5 Elution of the drugs CFT and SUL up to 42 days in contact with PBS at 37°C for 50P and 60P samples

kinds of samples, the rate was subsequently dropped down up to 4th day and subsequently the release become very very slow which continued up to 42 days. Faster drug release was observed for 50P samples owing to its lower pore surface area and its granular microstructure distribution of pores. Similar trend was observed for 60P samples however it had slower rate of drug release. On the other

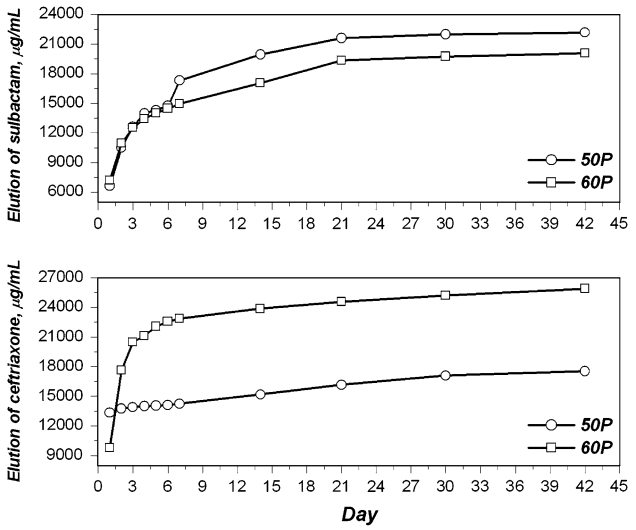

Fig. 6 Elution of the drugs CFT and SUL up to 42 days in contact with SBF at 37°C for 50P and 60P samples

hand, in contact with SBF, higher releases of both the drugs were observed in the total study period (Fig. 6) of 42 days. Percent drug yield on an average was found to be ~51 and 84.6% for 50P and 60P samples respectively. There was higher burst release of the individual drugs in the first day (13.35 and 9.78 mg/ml CFT and 6.66 and 7.2 mg/ml SUL from 50P and 60P samples respectively) in contact with SBF, but the rate of release was very uniform until 42 days. After 42 days, higher CFT release was observed for 60P samples than 50P samples while SUL showed the release rate close to each other. PBS had less effect on the drug elution rate for all the samples than SBF. In general, the elution rate of the drug CFS was much higher throughout the study period for SBF than PBS.

3.5 Bacterial colony counts at various sampling points

For group I samples, the organisms were gram-positive coccid arranged in single or diploid similar to the organism inoculated. No bacterial growth of *S. aureus* was found for group II; group III after 21 and 42 days post-implantation of CFS impregnated bioactive glass.

3.6 Histopathological examination

Histological section on 12 days in group I revealed osteomyelitic changes characterized by degenerative changes of haemopoigenesis centre, degeneration of osteophytes, fat cells along with mild fibrovascular proliferation of connective tissue. Bone marrow in the peripheral region showed infiltration with mononuclear cells and osteoclast (Fig. 7a). The histological features on 21 days (Fig. 7b) and 42 days

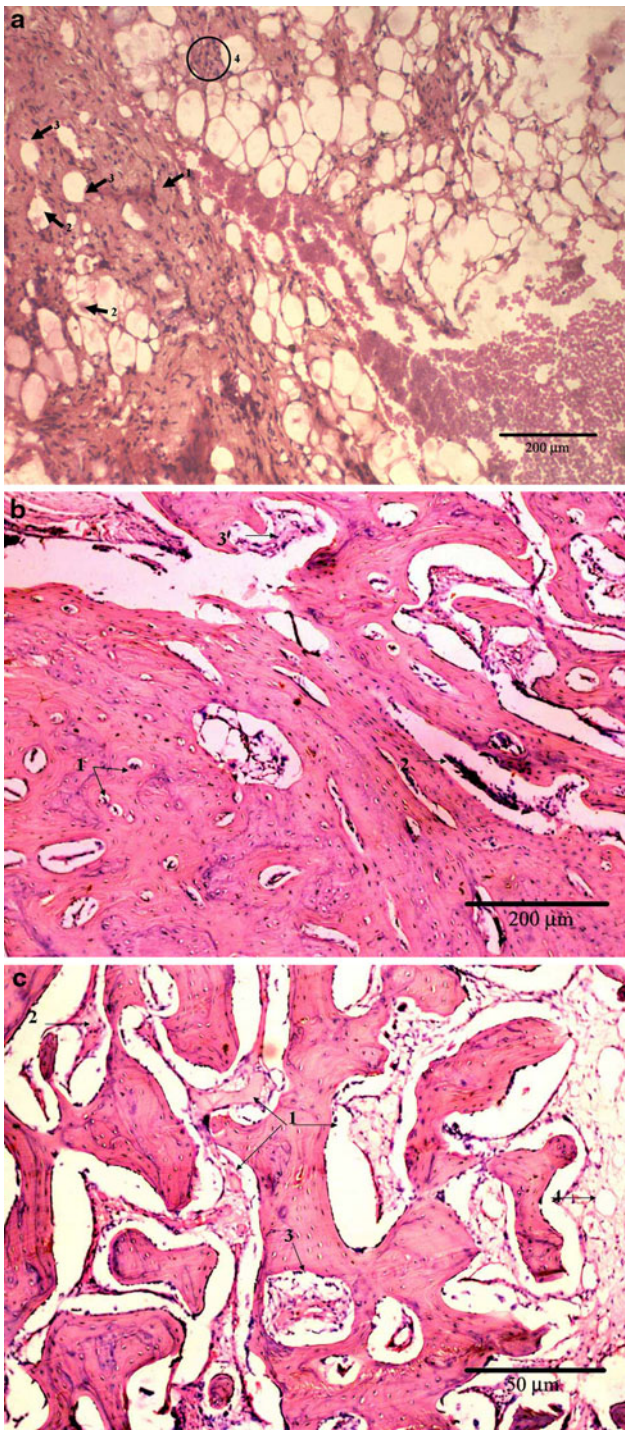

Fig. 7 Histopathology of group I taken after **a** 12 days, **b** 21 days and **c** 42 days post-operatively. **a** Degeneration of osteoblast indicating osteomyelitis (HE ×220); (1) Bony matrix, (2) osteocyte, (3) osteoclast and (4) immature bony osteoid. **b** Proliferating osteoblastic activity in Haversian canal (1); osteoclasts (2); supervening edema and cellular infiltration (3) (HE ×20). **c** Vascular proliferation in and around Haversian canal and canalicular spaces (1); scanty RBCs (2); cells (3) and some vacuolation in the osteoblastic stroma (4) indicates acute phase of osteomyelitis (HE ×220)

(Fig. 7c) were more intensified and aggressive in terms of osteomyelitic changes. Sections taken on 12 days from group II showed fibropurullent reaction with mucin deposit and presence of polymorphonuclear cells. Some portion of medulla was replaced by cellular clumps of mononuclear cells with eosinophilic exudation. This section was featured with chronic infection characterized by scanty vascularity of the cortico-medullary junction and presence of giant cells (Fig. 8a). The section of 21 days showed a degenerative stage of bony lamina with scanty cellular reaction and evidence of exudation with edematous fluid. The other structures were indistinct (Fig. 8b). Retained Haversian system with moderate parenchymal vascularity and formation of partial callus around the osteoid was evidenced on 42nd day section (Fig. 8c). On the other hand, histological section in group III on day 12 (Fig. 9a), illustrated the architectural details of bony laminae showing regenerative reaction, including exudation and mild cellular infiltration. Deposition of osteoids around the corner of Haversian canals was marked. The section on 21 days (Fig. 9b) showed a marked angiogenesis, characterized by haemorrhagic exudation and few osteoclasts. Proliferation of fibrocartilaginous structures in different directions was well marked. The section on 42 days (Fig. 9c) showed moderately repaired bony architectures characterized by proliferating osteoblasts and osteoclasts clustering all through the bony parenchyma. Few laminar portions showed mild degenerative changes with osteoclastic activity. The same observations analyzed quantitatively for different cellular events mentioned earlier, a score sheet were prepared and given in Table 4 alongwith the statistical analyses in Table 5.

3.7 Radiological examination

Induction of osteomyelitis was successful in animals of all groups following inoculation of *S. aureus* as evidenced by periosteal reaction and radiodense lamellated new bone formation. Lytic changes and thinning of bony cortex were evident. Prominent endosteal reaction with more radiodense bone marrow was visible. Both the osteophytic and lytic changes were suggestive of osteomyelitis (Fig. 10).

In group II animals, the radiograph on 12 days showed increased radio-opacity along with loss of characteristics of cancellous bone in proximal metaphysis of tibia (Fig. 11a). Both the phytic and lytic changes were prominent in proximal metaphysis. Formation of new bone was of amorphous type. Moderate endosteal reaction was clearly visible. Anterior cortical border of proximal metaphysis of tibia showed discontinuation in some places. Epiphyseal cartilage showed secondary osteophytic changes. The radiograph on 21 days showed variable radiodensity in

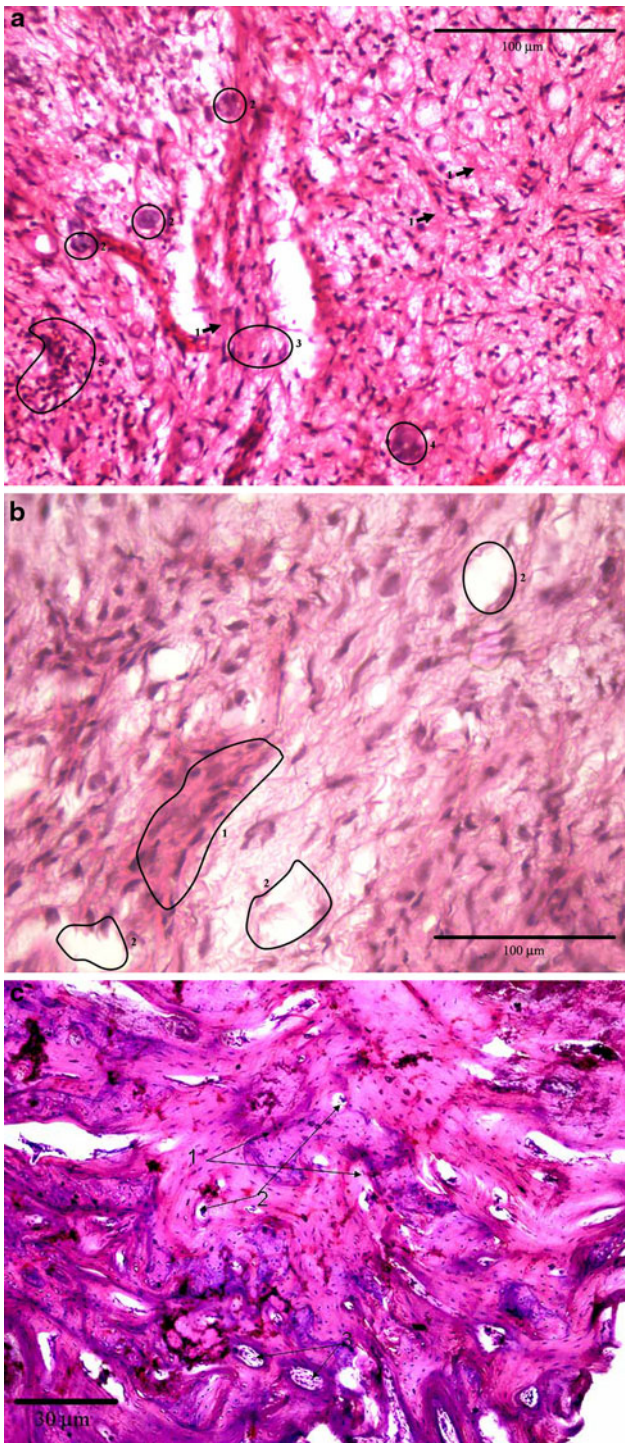

Fig. 8 Histopathology of group II taken after **a** 12 days, **b** 21 days and **c** 42 days post-operatively. **a** Fibropurullent reaction with mucin deposit (1) and presence of polymorphonuclear cells (2); eosinophilic exudation (3); presence of giant cells (4) indicate the chronicity of the disease (5) (HE ×220). **b** Degenerative stage of bony lamina (1) with scanty cellular reaction; Evidence of exudation with edematous fluid (2) (HE ×240). **c** Formation of partial callus around the osteoid (1); Haversian system (2) retains their structures. Vascularity of the bony parenchyma is moderate (3) (HE ×210)

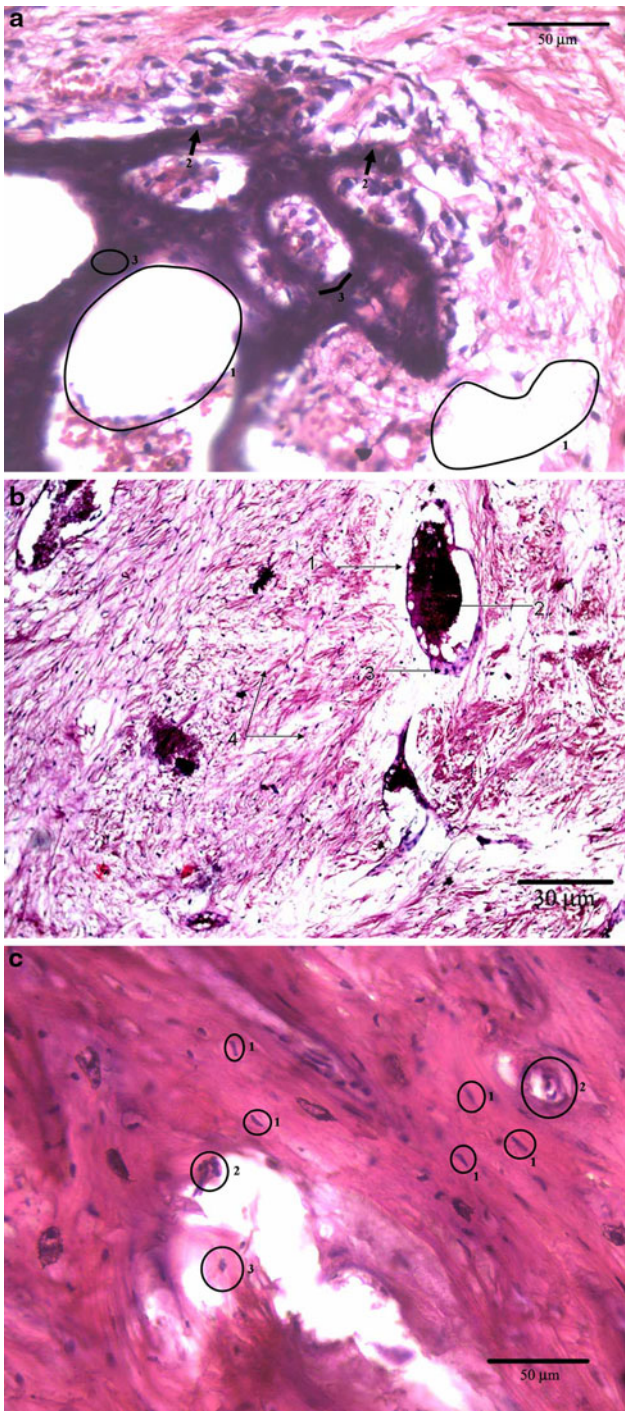

◀ **Fig. 9** Histopathology of group III taken after **a** 12 days, **b** 21 days and **c** 42 days post-operatively. **a** Architectural details of bony laminae showing regenerative reaction including exudation (1) and mild cellular infiltration (2); deposition of osteoids (3) around the corner of Haversian canals are marked (HE ×240). **b** Marked angiogenesis (1) characterized by haemorrhagic exudation (2) of RBCs with fibrin and few scavenger cells; osteoclasts (3). Proliferation of fibrocartilaginous structures (4) in different directions are well marked (HE ×210). **c** Moderately repaired bony architectures characterized by proliferating osteoblasts (1) and osteoclasts (2) clustering all through the bony parenchyma. Few laminar portion shows mild degenerative changes (3) with osteoclastic activity (HE ×240)

anterior border of proximal metaphysis along with discontinuation of cortex in few places (Fig. 11b). Endosteal reaction was mild. Reestablishment of the medullary cavity and remodelling of cortex were noticeable. On day 42, radiograph showed few radiolucent zones characteristic of osteoclastic changes. Absence of periosteal and endosteal reaction, reestablishment of medullary cavity along with cortical continuation demonstrated the radiograph as under process of healing (Fig. 11c).

Table 4 Score sheet prepared for different cellular events after observing the histological images for all groups of animals

Category	(i)	(ii)	(iii)	(iv)	(v)	(vi)	(vii)	(viii)	Total score
Gr. I—12 days	1	1	2	1	3	4	3	4	19
Gr. I—21 days	1	2	1	1	3	3	2	4	17
Gr. I—42 days	1	2	1	1	2	3	2	3	15
Gr. II—12 days	3	3	2	4	2	1	3	2	21
Gr. II—21 days	3	2	2	4	4	4	2	4	25
Gr. II—42 days	4	4	3	4	4	4	2	4	29
Gr. III—12 days	3	3	3	3	4	4	3	4	27
Gr. III—21 days	3	4	3	3	4	4	3	4	28
Gr. III—42 days	3	4	4	3	4	4	3	4	29

(i) Degenerative changes; (ii) fibro-vascular proliferation; (iii) infiltration with mononuclear cells; (iv) osteoclastic activity; (v) fibropurullent reaction; (vi) mucin deposit; (vii) vascularity; (viii) presence of giant cells

Table 5 Statistical analyses based on the results of Table 4

	12 days	21 days	42 days
Gr. I	$19^{a} \pm 0.58$	$17^{a} \pm 0.58$	$15^{a} \pm 0.58$
Gr. II	$21^{b} \pm 0.58$	$25^{b} \pm 0.58$	$29^{b} \pm 0.58$
Gr. III	$27^{c} \pm 0.58$	$28^{c} \pm 0.58$	$29^{b} \pm 0.58$

Means having different superscripts differ significantly at 5% level

In group III on day 12 (Fig. 12a) radiograph showed unabsorbed antibiotic impregnated bioactive glass in proximal metaphysis of tibia. Continuation of periosteum and characteristic appearance of spongy bone with establishment of medullary cavity is restored suggesting remodeling. The focus of inoculation is evident as radiolucent small circular area on the proximal metaphysis. Lateral radiograph on 21 days (Fig. 12b) showed unaltered radiodense antibiotic impregnated bioactive glass block in proximal metaphysis of tibia. Continuation of periosteum with appearance of characteristic metaphyseal bone is clearly established. Endosteal reaction is not evident. Periosteal reaction is

radiographically absent. Radiodensity in and around the antibiotic impregnated block is comparatively more than other area proximal metaphysis. Lytic changes are not viewed. Remodeling of bone is appeared to be nearly to complete. Radiograph on 42 days (Fig. 12c) of tibia–fibula showed rectangular shaped intact radiodense antibiotic impregnated block at proximal metaphysis of tibia. Metaphyseal region showed complete disappearance of radiodense hard tissue aggregation as observed in the early days of osteomyelitis along with complete establishment of continuation of periosteum. Radiodensity of medullary cavity as well as cortical bone was homogenous to that of unaffected diaphyseal bony tissue. As before, score sheet prepared observing different bony events are presented in Table 6 with statistical analyses in Table 7.

Fig. 10 Radiograph of tibia–fibula of group I animals after 42 days

3.8 In vivo drug concentration

In vivo, initial high release of both CFT and SUL were observed in bioactive glass implanted group (group III) as compared to group II in bone and serum on day 12 followed by decrease in concentration (in bone) on days 21 and 42 for group III animals (Fig. 13). Parenteral therapy (group II) maintained the drug concentration almost constant throughout the study period although very close to the MIC values (in bone). SUL concentration in group II animals showed almost similar and constant drug release in the observed days (12, 21 and 42), again very close to MIC. On the contrary, both drug concentrations were found to be almost constant in serum for group III animals through the study period and the values were almost 15 times higher than the MIC of *S. aureus* (Fig. 13a, b).

3.9 SEM of the extracted cortical bone

Microstructures of bone defect sites for all the group of animals are given in Fig. 14a–d. Figure 14a and b display the status of bone after 42 days when no treatment was provided (group I) after development of osteomyelitis (i.e. control) and the site when parenterally treated (group II) by CFS, respectively. Figure 14c and d portray the status of bone after 21 and 42 days when implanted with drug loaded porous bioactive glass implants (group III). It was

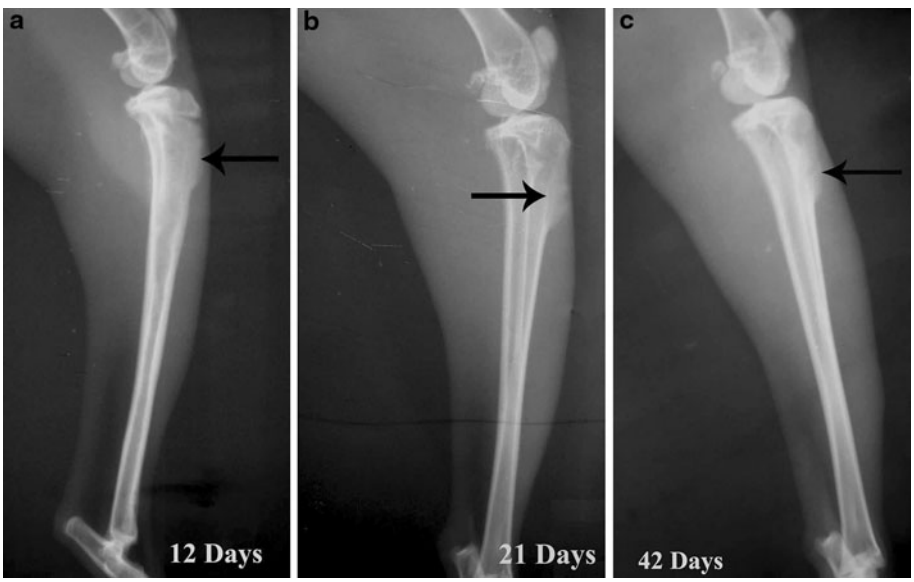

Fig. 11 Radiographs of tibia–fibula of group II animals after **a** 12 days, **b** 21 days and **c** 42 days

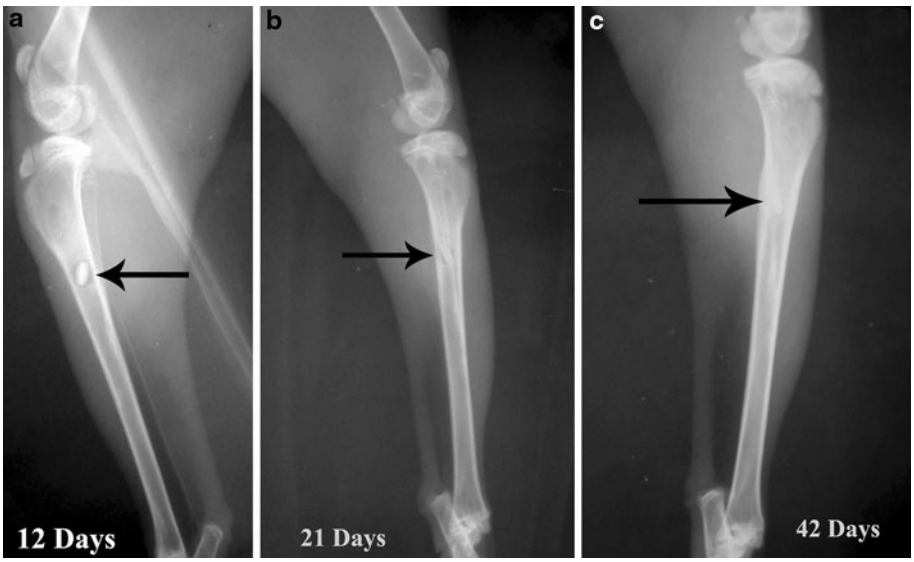

Fig. 12 Radiographs of tibia–fibula of group III animals after **a** 12 days, **b** 21 days and **c** 42 days

Table 6 Score sheet prepared observing different bony events of radiology images in all groups of animals

Category	Periosteal reaction	Radiodensity	Visible bone defect	Resorptive changes	Cortical continuity	Endosteal reaction	Total score
Gr. I—12 days	1	3	1	1	1	1	8
Gr. I—21 days	1	3	1	1	1	1	8
Gr. I—42 days	1	3	1	1	1	1	8
Gr. II—12 days	2	3	2	1	1	2	11
Gr. II—21 days	3	3	3	2	2	3	16
Gr. II—42 days	4	3	4	3	4	4	22
Gr. III—12 days	3	3	3	4	4	3	20
Gr. III—21 days	4	4	4	4	4	4	24
Gr. III—42 days	4	4	4	4	4	4	24

Table 7 Statistical analyses based on the results of Table 6

	12 days	21 days	42 days
Gr. I	$8^{a} \pm 0.58$	$8^{a} \pm 0.58$	$8^{a} \pm 0.58$
Gr. II	$11^{b} \pm 0.58$	$16^{b} \pm 0.58$	$22^{b} \pm 0.58$
Gr. III	$20^{c} \pm 0.58$	$24^{c} \pm 0.58$	$24^{c} \pm 0.58$

Means having different superscripts differ significantly at 5% level

observed that after 42 days in group I, there was abundance of RBC cells together with decalcification of the bony matrix, indicative of osteolytic activity of the *S. aureus* at the control site. There was recognizable presence of bridging callus and fibrocartilaginous tissues but absence of mature bone cells formation after parenteral treatment of 42 days. On the other hand, drug incorporated porous bioactive glass scaffolds showed reticulo formation of collagenous structure and penetration of bony trabeculae into the porous structure by 21 days and complete absence of any RBC cells indicating faster bone mineralization with no reincarnation of the bacteria at the defect site. However, by 42 days, matured bone could not cover the defect site. Inside of such implant, there were still some abstract collagenous tissues, indicating bone mineralization process was continuing at the inside.

4 Discussion

Jones et al. varied sintering temperature to fabricate porous bioactive glass and found a very simple and effective way of controlling the texture of the gel-glass foams to control the ion release for gene stimulation as long as the scaffold is a glass [21]. They also found that changing the textural porosity of the foams had an effect on the dissolution of the scaffolds and accordingly suggested for sintering the bioactive glass composition below 800°C. The same justification is also applied in the present investigation.

Due to lower quantity of naphthalene in the 50P green matrix and closer particle compaction, after drying, micropores were predominant in the sample after sintering owing to its further shrinkage. This was not the case for

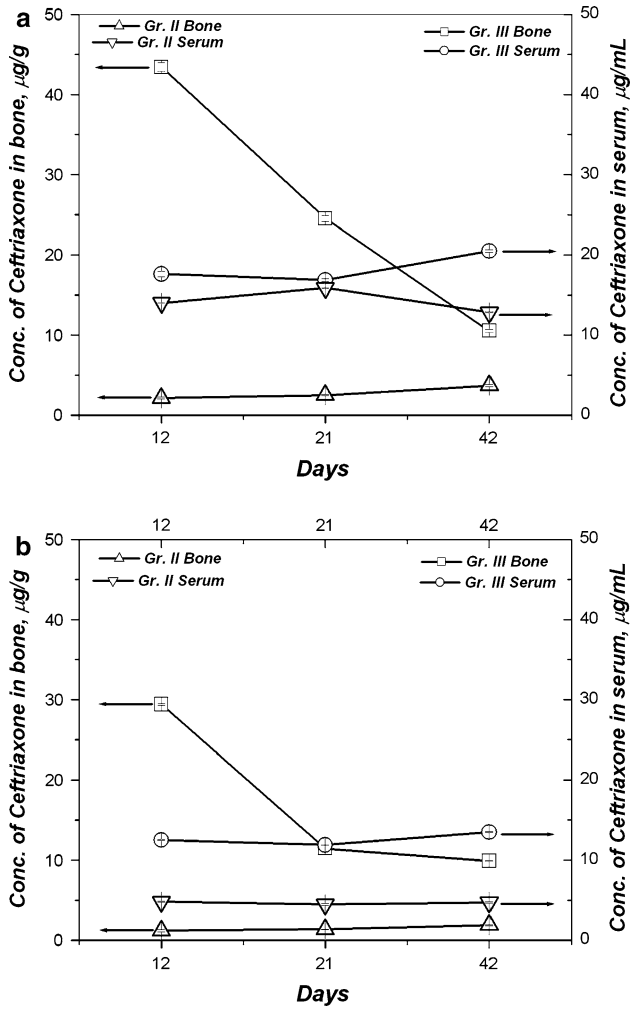

Fig. 13 In vivo concentration of **a** ceftriaxone sodium and **b** sulbactam sodium in different groups over different days interval found in bone and serum (group II: parenteral injection of antibiotic and group III: CFS impregnated bioactive glass implanted group)

60P; it had more quantity of naphthalene, less close particle contact in the green state after drying and a good distribution of macro- and micropore in the matrix after sintering. 50P sample also showed some disruption of the microstructure which may be due to the uneven shrinkage of both pore and glass particles during sintering. 50P samples consisted of micropores, which also influenced poorer drug loading. Macropores (>50 μm) are of an appropriate scale to influence tissue function, for example, pores greater than 300 μm in size are typically recommended as optimal for bone in-growth in relation to vascularization of the construct. Micropores (<50 μm) are of a scale to influence cell function (e.g., cell attachment) given that mammalian cells typically are 10–20 μm in size. Nanoporosity refers to pore architectures or surface textures on a nano scale (1–1000 nm) [22, 23]. There are reports on efficacy of mesoporous special bioactive glass with good bone bonding ability which, when used for a local drug delivery system could not elute the drug for a prolonged period of time, most probably due to this mesoporosity and poor interconnectivity. Only mesopore or micropore cannot elute the drug in a systematic and prolonged manner. The reason of course is obvious. Drug adsorption efficiency is poor for nanopore or mesopore while macropore cannot hold the drug in the physiological fluid. Depending on the composition, some of the drug molecules attached through secondary bonding mostly on the surface and to a lesser extent inside the mesopore channel and hence faster drug elution in PBS/SBF [24]. There are some specific distributions of pore, which can serve the purpose. Apart from the chemical interaction between the drug moiety and bioactive glass composition, surface charge in aqueous medium also had a role to play for CFT and SUL adsorption inside bioactive glass pore channels. To the best of our knowledge, there is no report on this parameter w.r.t. drug adhesion on this glass surface. Surface charge of this particular material decreases from the as-prepared condition in different pH condition. Further, lower surface charge cannot adsorb a significant loading of drug at the physiological pH condition (−21.7 mV in this case). It is being negative zeta potential, all the cations would be exposed on the surface surrounded by a negatively charged Stern layer. As the zeta potential becomes gradually more and more negative, more numbers of cations are exposed on the surface, which can interact with the anionic part of the drug molecule with a consequent increase in drug loading. An ideal local drug delivery system which can elute the drug for a very prolonged time should have either higher surface charge and/or scaffold should be designed in a manner so that it contains both micro- and macropore (i.e. bimodal distribution of pore) [25]. Due to these reasons, mesoporous scaffolds had poor drug loading efficiency [24, 26]. Due to the same reason, in the present study, distribution of CFS in 50P porous scaffold as evidenced from Fig. 4, was not homogenous. From the chemical structure of CFS molecule, it was understood that −COOH group interacted with glass network former. However, the binding capacity of the drug to the biomaterial is an import factor to retard the drug release [27]. From the surface charge point of view, both 50P and 60P samples should adsorb with lower efficiency but due to bimodal distribution of both micro- and macropore, 60P samples had a higher drug loading efficiency.

In contact with PBS, 50P samples eluted both CFT and SUL much faster than the 60P sample. Since PBS was unreactive with the bioactive glass matrix, drug elution was fastest in contact with it. Again, due to bimodal distribution of micro- and macropore, 60P samples eluted slower in contact with PBS. On the other hand, SBF was reactive to the bioactive glass matrix. Hench was first who proposed

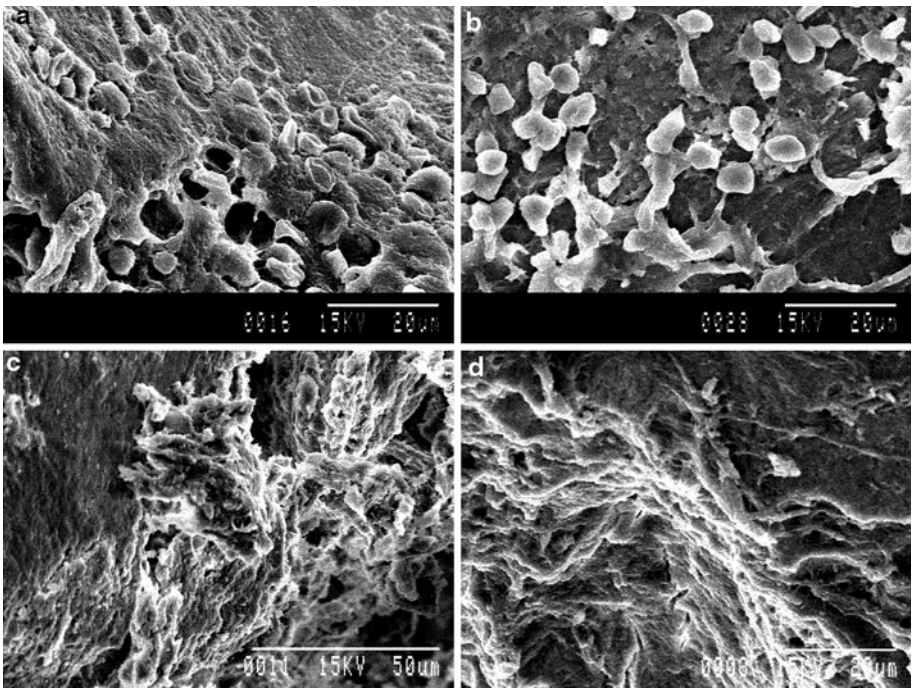

Fig. 14 SEM photomicrograph of the extracted bone for the samples of **a** group I animal after 42 days, **b** group II animal after 42 days and **c**, **d** group III animal after 21 and 42 days, respectively

that bioactive glass undergoes the steps including rapid exchange of Na^+ or K^+ with H^+ or H_3O^+ from SBF, loss of soluble silica in the form of $Si(OH)_4$ at the glass-solution interface, condensation and repolymerization of a silica-rich layer, ultimately forming a carbonated calcium phosphate layer on the bioactive glass surface [28]. This layer becomes matured with due course of time. In the initial days, dissolution of both Ca^{2+} and PO_4^{3-} were predominant and after that, deposition of calcium phosphate starts. Due to this, elution rates of CFT and SUL were faster in contact with SBF like the PBS in the initial stage. However, the rate decreased after 6 days due to initiation of deposition of calcium phosphate phase. Zhao et al. [26] pointed out that CaO content in bioactive glass composition influence the release kinetics because of the chelation between the drug and the calcium species. Our observation also corroborate the same finding, where we have seen that the rate of drug release was very uniform with time. The more pronounced burst release of drugs in PBS than SBF may be attributed to the above stated reasons. Similar observation was also noticed by Rai et al., who demonstrated that SBF-soaked composites of polycaprolactone-tricalcium phosphate had delayed release of biomolecules and absence of total release in the total study period [29].

Finally, from the above observations we had selected the 60P samples for further animal trial owing to its 60–65% porosity (bimodal) with an average pore size $\sim$60 μm, having higher interconnectivity, moderately high CFS adsorption efficiency ($\sim$49%) and finally with much slower, prolonged and homogeneous elution profile up to 42 days (higher than the MIC values) in contact with SBF.

Now, as far as the animal trial is concerned, previous histological findings on biodegradable implants demonstrated that infection was subsided by 3 weeks and 6 weeks and inflammatory cells were replaced with bone forming cells upon treatment of osteomyelitis [8, 30–32]. Histopathology and microbiology are the best evidence of treatment efficiency in osteomyelitis [33]. Besides, histological observations provide more detailed knowledge about the cellular events during incorporation of different types of ceramic implants. In this study, from acceptability of the implant and effective delivery of the antibiotic to osteomyelitic bone confirmed the minimal reaction towards biomaterial and gradual new bone formation in the area. From radiology, it was shown that initial bacterial colonization progressing with inflammation, hyperaemia, formation of abscess [34], production of purulent exudates entering the cortical bone via Haversian and Volkmann's canals ultimately leads to necrosis of bone fragments and development of osteomyelitis. The treatment of osteomyelitis in orthopaedic surgery poses a great challenge. Due to inherent characteristic of bony tissue, the success of treatment of osteomyelitis, even with different highly sensitive antibiotics, are very limited that may be mastered with local effective antibiotic delivery with desired concentration. In group III animals, newly grown periosteal bone was predominant suggesting bone healing and remodelling that might be due to the desired level of antibiotic concentration at the site controlling the infection. Further, the results of statistical analyses of both histopathology and radiology with time showed that there was significant difference exist between the different groups of

animals at a given time but not within the groups at different time interval. Different implantable delivery system having similar radiographic features of implant with well toleration and gradual new bone formation have been investigated [5, 30, 32]. The present study design had certain limitations too. An additional experimental group of animals that received combined local and short-term systemic antimicrobial treatment would have served as a group in which the comparison of efficacy of present research methodologies of treating osteomyelitis can be best judged. Yet, for comparison, a group of animals that received systemic antimicrobial treatment alone for the whole 6-week treatment period has been made in the present article, which would also have given a reference for efficacy in comparison with that of traditional systemic treatment.

The efficacy of systemically applied antibiotic for precluding osteomyelitis seems to be very poor duo to impermeability of this antibiotic in attaining desirable concentration at the target site due to blood-bone barrier [35]. The administration of antibiotics for 4–6 weeks is usually recommended for the treatment of chronic osteomyelitis [36, 37]. The local antibiotic treatment may use the blood-bone barrier effectively as a protection of the body against a very high local antibiotic concentration without systemic side effects [38]. In the present study, the reason for the efficacy of this bioactive glass composition in the treatment of osteomyelitis is probably the advantageous pharmacokinetics at the site of infection. The pharmacokinetics of the composites in vivo showed that therapeutic concentration of antibiotic was maintained at the site of implantation, which was adequate to provide antimicrobial activity. The MIC of CFS against *S. aureus* is 1 mg/l [39]. The results clearly indicate the superiority of these bioactive glass based implants in maintaining higher concentrations of antibiotics at the site than the multi-dose parenteral (2 injections a day for 6 weeks including cost and chances of systemic toxicity). Compared with similar biodegradable antibiotic releasing bone grafts, potentiality of this biomaterial is paramount considering maintenance of implant integrity and release of antibiotic at an adequate concentration. Normally, first order release is not desired and generally a constant release rate is expected by the researchers. However, an early burst could actually be quite useful in the initial treatment of the microorganisms at the infection site, and the later, lower rate of release, could maintain the medium sterile.

From the SEM study of the bone-biomaterial interface of all groups also, it was found that group III animals had better bone ingrowth into the deep pores through the interpore connections after 21 days, which became matured at day 42. These findings also corroborated our previous finding about porous bioactive glass which had bone in-growth into the deep pores [11]. Intra-implant vascularization for group III animals' cortical site after 21 days had a favourable gradient for draining out of the drug CFS through capillary of the bone tissue, which was occurring even after 42 days, and meanwhile the new bone on the surface became matured and there was sign of further bone mineralization process subsurface. This finding also corroborated the findings of Castro et al. [40].

5 Conclusion

In this study, a rational approach was made to combine drugs irreversible β-lactamase inhibitor and β-lactam antibiotic with a special bioactive glass matrix, which can deliver the drug locally and sustainably. Two kinds of pore percentage with differing distribution of pores sizes were used. It was recognized that higher pore percentage with a distribution of macro- to micropores were found to be more efficient for prolonged time drug elution both in vitro and in vivo compared to the data available for mesoporous scaffolds. The criteria was matched with 60P samples which had 60–65% porosity (bimodal) with an average pore size $\sim$60 μm, having higher interconnectivity, moderately high CFS adsorption efficiency ($\sim$49%). CFS release from the implants was much faster in PBS compared to in contact with SBF. Both the results of in vitro and in vivo drug elution after 42 days showed drug release at least 10–15 times higher than minimum inhibitory concentration of CFS against *S. aureus* compared to parenteral treatment (2 injections a day for 6 weeks). In vivo drug pharmacology and SEM on bone-implant and/or defect interface also proved the superiority of CFS loaded porous special bioactive glass implants than parenteral group based on eradication of infection and new bone formation, which could be safely applied for treatment of chronic osteomyelitis patient of animal and human subjects.

Acknowledgments The authors wish to express their sincere thanks for the financial support by Department of Science and Technology, India [T.1 (7)/TIFA/2006-CGCRI] and the Director, CGCRI, India and Vice Chancellor, West Bengal University of Animal and Fishery Sciences, Kolkata, India for their generous and kind support to this work. All the personnel related to the characterization of the materials are sincerely acknowledged.

References

1. Walenkamp GHIM. Chronic osteomyelitis. Acta Orthop Scand. 1997;68(5):497–506.
2. Mader JT, Landon GC, Calhoun J. Antimicrobial treatment of osteomyelitis. Clin Orthop Relat Res. 1993;295:87–95.
3. Kanellakopoulou K, Giamarellos-Bourboulis EJ. Carrier systems for the local delivery of antibiotics in bone infections. Drugs. 2000;59(6):1223–32.

4. Soundrapandian C, Datta S, Sa B. Drug-eluting implants for osteomyelitis. Crit Rev Ther Drug Carrier Syst. 2007;24(6): 493–545.
5. Nandi SK, Mukherjee P, Roy S, Kundu B, De DK, Basu D. Local antibiotic delivery systems for the treatment of osteomyelitis—a review. Mater Sci Eng C. 2009;29(8):2478–85.
6. Giavaresi G, Borsari V, Fini M, Giardino R, Sambri V, Gaibani P, et al. Preliminary investigations on a new gentamicin and vancomycin-coated PMMA nail for the treatment of bone and intramedullary infections: an experimental study in the rabbit. J Orthop Res. 2008;26(6):785–92.
7. Kundu B, Soundrapandian C, Nandi SK, Mukherjee P, Dandapat N, Roy S, et al. development of new localized drug delivery system based on ceftriaxone–sulbactam composite drug impregnated porous hydroxyapatite: a systematic approach for in vitro and in vivo animal trial. Pharm Res. 2010;27(8):1659–76.
8. Nandi SK, Kundu B, Ghosh SK, Mandal TK, Datta S, De DK, et al. Cefuroxime-impregnated calcium phosphates as an implantable delivery system in experimental osteomyelitis. Ceram Int. 2009;35(4):1367–76.
9. Hing KA. Bioceramic bone graft substitutes: influence of porosity and chemistry. Int J Appl Ceram Technol. 2005;2(3):184–99.
10. Mader JT, Shirtliff ME, Bergquist SC, Calhoun J. Antimicrobial treatment of chronic osteomyelitis. Clin Orthop Relat Res. 1999;360:47–65.
11. Nandi SK, Kundu B, Datta S, De DK, Basu D. The repair of segmental bone defects with porous bioglass: an experimental study in goat. Res Vet Sci. 2009;86(1):162–73.
12. Bharati S, Soundrapandian C, Basu D, Datta S. Studies on a novel bioactive glass and composite coating with hydroxyapatite on titanium based alloys: effect of γ-sterilization on coating. J Eur Ceram Soc. 2009;29(12):2527–35.
13. Caron F, Gutmann L, Bure A, Pangon B, Vallois JM, Pechinot A, et al. Ceftriaxone–sulbactam combination in rabbit endocarditis caused by a strain of Klebsiella pneumoniae producing extended-broad-spectrum TEM-3 beta-lactamase. Antimicrob Agents Chemother. 1990;34(11):2070–4.
14. Foulds G, Stankewich JP, Marshall DC, O'Brien MM, Hayes SL, Weidler DJ, et al. Pharmacokinetics of sulbactam in humans. Antimicrob Agents Chemother. 1983;23(5):692–9.
15. Ghosh SK, Nandi SK, Kundu B, Datta S, De DK, Roy SK, et al. In vivo response of porous hydroxyapatite and beta-tricalcium phosphate prepared by aqueous solution combustion method and comparison with bioglass scaffolds. J Biomed Mater Res. 2008;86(1):217–27.
16. Kundu B, Sinha MK, Mitra MK, Basu D. Fabrication and characterization of porous hydroxyapatite ocular implant followed by an in vivo study in dogs. Bull Mater Sci. 2004;27(2):133–40.
17. Hench LL. The story of Bioglass®. J Mater Sci: Mater Med. 2006; 17(11):967–78.
18. Hasegawa M, Sudo A, Komlev VS, Barinov SM, Uchida A. High release of antibiotic from a novel hydroxyapatite with bimodal pore size distribution. J Biomed Mater Res. 2004;70(2):332–9.
19. Kokubo T, Kushitani H, Sakka S, Kitsugi T, Yamamuro T. Solutions able to reproduce in vivo surface-structure changes in bioactive glass–ceramic A–W. J Biomed Mater Res. 1990;24(6): 721–34.
20. Norden CW. Experimental osteomyelitis. I. A description of the model. J Infect Dis. 1970;122(5):410–8.
21. Jones JR, Ehrenfried LM, Hench LL. Optimising bioactive glass scaffolds for bone tissue engineering. Biomaterials. 2006;27(7): 964–73.
22. Gibson LJ, Ashby MF. Cellular solids: structure and properties. 2nd ed. Cambridge: Cambridge University Press; 1997.
23. D883-99. Standard terminology relating to plastics. American Standard for Testing and Methods. ASTM; 1999.
24. Zhu Y, Kaskel S. Comparison of the in vitro bioactivity and drug release property of mesoporous bioactive glasses (MBGs) and bioactive glasses (BGs) scaffolds. Microporous Mesoporous Mater. 2009;118(1–3):176–82.
25. Komlev VS, Barinov SM, Koplik EV. A method to fabricate porous spherical hydroxyapatite granules intended for time-controlled drug release. Biomaterials. 2002;23(16):3449–54.
26. Zhao YF, Loo SC, Chen YZ, Boey FY, Ma J. In situ SAXRD study of sol–gel induced well-ordered mesoporous bioglasses for drug delivery. J Biomed Mater Res A. 2008;85(4):1032–42.
27. Burgos AE, Belchior JC, Sinisterra RD. Controlled release of rhodium (II) carboxylates and their association complexes with cyclodextrins from hydroxyapatite matrix. Biomaterials. 2002;23(12):2519–26.
28. Hench LL. Bioceramics: from concept to clinic. J Am Ceram Soc. 1991;74(7):1487–510.
29. Rai B, Teoh SH, Ho KH. An in vitro evaluation of PCL–TCP composites as delivery systems for platelet-rich plasma. J Control Release. 2005;107(2):330–42.
30. Itokazu M, Ohno T, Tanemori T, Wada E, Kato N, Watanabe K. Antibiotic-loaded hydroxyapatite blocks in the treatment of experimental osteomyelitis in rats. J Med Microbiol. 1997;46(9): 779–83.
31. Korkusuz F, Korkusuz P, Eksioglu F, Gursel I, Hasirci V. In vivo response to biodegradable controlled antibiotic release systems. J Biomed Mater Res. 2001;55(2):217–28.
32. Sanchez E, Baro M, Soriano I, Perera A, Evora C. In vivo–in vitro study of biodegradable and osteointegrable gentamicin bone implants. Eur J Pharm Biopharm. 2001;52(2):151–8.
33. Joosten U, Joist A, Frebel T, Brandt B, Diederichs S, von Eiff C. Evaluation of an in situ setting injectable calcium phosphate as a new carrier material for gentamicin in the treatment of chronic osteomyelitis: studies in vitro and in vivo. Biomaterials. 2004; 25(18):4287–95.
34. Woodward JC, Riser WH. Morphology of fracture non union and osteomyelitis. Vet Clin North Am Small Anim Pract. 1991;21: 313–44.
35. Barza M. Anatomical barriers for antimicrobial agents. Eur J Clin Microbiol Infect Dis. 1993;12(Suppl 1):31–5.
36. Gordon L, Chiu EJ. Treatment of infected non-unions and segmental defects of the tibia with staged microvascular muscle transplantation and bone-grafting. J Bone Joint Surg. 1988;70(3): 377–86.
37. Calhoun J, Mader JT. Antibiotic beads in the management of surgical infections. Am J Surg. 1989;157(4):443–9.
38. Walenkamp GHIM, Vree TB, Van Rens TJG. Gentamicin-PMMA beads: pharmacokinetic and nephrotoxicological study. Clin Orthop Relat Res. 1986;205:171–83.
39. Shrivastava SM, Saurabh S, Rai D, Dwivedi VK, Chaudhary M. In vitro microbial efficacy of sulbactomax: a novel fixed dose combination of ceftriaxone sulbactam and ceftriaxone alone. Curr Drug Ther. 2009;4(1):73–7.
40. Castro C, Sanchez E, Delgado A, Soriano I, Nunez P, Baro M, et al. Ciprofloxacin implants for bone infection. In vitro-in vivo characterization. J Control Release. 2003;93(3):341–54.